

Origin of itinerant ferromagnetism in two-dimensional Fe_3GeTe_2

Xi Chen(陈熙), Zheng-Zhe Lin(林正喆), and Li-Rong Cheng(程丽蓉)

Citation: Chin. Phys. B, 2021, 30 (**4**): 047502. DOI: 10.1088/1674-1056/abd164
Journal homepage: http://cpb.iphy.ac.cn; http://iopscience.iop.org/cpb

What follows is a list of articles you may be interested in

Crystal structure and electromagnetic responses of tetragonal GdAlGe

Cong Wang(王聪), Yong-Quan Guo(郭永权), Tai Wang(王泰), and Shuo-Wang Yang(杨硕望)
Chin. Phys. B, 2020, 29 (**12**): 127502. DOI: 10.1088/1674-1056/abad25

Spin waves and transverse domain walls driven by spin waves: Role of damping

Zi-Xiang Zhao(赵梓翔), Peng-Bin He(贺鹏斌), Meng-Qiu Cai(蔡孟秋), Zai-Dong Li(李再东)
Chin. Phys. B, 2020, 29 (**7**): 077502. DOI: 10.1088/1674-1056/ab90e5

Discrete modulational instability and bright localized spin wave modes in easy-axis weak ferromagnetic spin chains involving the next-nearest-neighbor coupling

Jiayu Xie(谢家玉), Zhihao Deng(邓志豪), Xia Chang(昌霞), Bing Tang(唐炳)
Chin. Phys. B, 2019, 28 (**7**): 077501. DOI: 10.1088/1674-1056/28/7/077501

Voltage control of ferromagnetic resonance and spin waves

Xinger Zhao(赵星儿), Zhongqiang Hu(胡忠强), Qu Yang(杨曲), Bin Peng(彭斌), Ziyao Zhou(周子尧), Ming Liu(刘明)
Chin. Phys. B, 2018, 27 (**9**): 097505. DOI: 10.1088/1674-1056/27/9/097505

Angle-dependent spin waves in antidot bilayers

Hu Chun-Lian, Liao Leng, Stamps R
Chin. Phys. B, 2014, 23 (**12**): 127501. DOI: 10.1088/1674-1056/23/12/127501

RAPID COMMUNICATION

Origin of itinerant ferromagnetism in two-dimensional Fe_3GeTe_2*

Xi Chen(陈熙), Zheng-Zhe Lin(林正喆)†, and Li-Rong Cheng(程丽蓉)

School of Physics and Optoelectronic Engineering, Xidian University, Xi'an 710071, *China*

(Received 21 September 2020; revised manuscript received 30 November 2020; accepted manuscript online 8 December 2020)

Magnetic order in two-dimensional systems was not supposed to exist at finite temperature. In recent years, the successful preparation of two-dimensional ferromagnetic materials such as CrI_3, $Cr_2Ge_2Te_6$, and Fe_3GeTe_2 opens up a new chapter in the remarkable field of two-dimensional materials. Here, we report on a theoretical analysis of the stability of ferromagnetism in Fe_3GeTe_2. We uncover the mechanism of holding long-range magnetic order and propose a model to estimate the Curie temperature of Fe_3GeTe_2. Our results reveal the essential role of magnetic anisotropy in maintaining the magnetic order of two-dimensional systems. The theoretical method used here can be generalized to future research of other magnetic two-dimensional systems.

Keywords: two-dimensional (2D) ferromagnetism, spin wave, magnetic anisotropy

PACS: 75.70.Ak, 75.10.Jm **DOI:** 10.1088/1674-1056/abd164

1. Introduction

Atomically thin two-dimensional (2D) crystals can present exceptional electronic structures as a result of reduced dimensionality. The success in 2D material research brings vast opportunities to pursue emerging physical properties. Various 2D crystals are discovered, ranging from semiconductors, highly correlated materials to superconductors. Recently, magnetic crystals are added to the 2D material family.[1–3] In particular, intrinsic ferromagnetism in 2D materials is a new form of condensed matter. Unlike the ferromagnetism in conventional ultrathin metals, ferromagnetic (FM) 2D materials hold magnetic order in reduced dimensionality and may exhibit new physics for spintronics.

With the rapid development, 2D materials have permeated into many research areas[4–9] and also bring opportunities for finding ferromagnetism in reduced dimensionality. Although the Mermin–Wagner theorem[10] asserts that 2D long-range FM order cannot exist in isotropic magnetic systems, a recent discovery has found 2D layered systems possessing intrinsic magnetocrystalline anisotropy against thermal fluctuations (e.g., CrI_3,[11–15] $Cr_2Ge_2Te_6$,[16] and $CrSiTe_3$[17]). However, the Curie temperatures of CrI_3, $Cr_2Ge_2Te_6$, and $CrSiTe_3$ are only dozens of Kelvin. In recent years, Fe_3GeTe_2 has been found to have a Curie temperature close to room temperature[18–25] (150–220 K depending on Fe occupancy). By the doping of the ionic gate, the Curie temperature of atomically thin Fe_3GeTe_2 is dramatically elevated to room temperature.[18,26] The discovery of Fe_3GeTe_2 provides a new chance for ultra-thin spintronics. Magnetically ordered 2D crystals open vast possibilities for novel physical phenomena and new device concepts.

The observation of long-range 2D magnetic order is significant for understanding the microscopic mechanism of magnetic anisotropy. The breaking of spin rotational symmetry can lead to dipolar interactions, single-ion anisotropy, and the anisotropy of the exchange interactions. For the case of strong single-ion anisotropy, Onsager predicted the existence of a magnetically ordered phase at finite temperature.[27] Furthermore, strong electron interactions in 2D systems are likely to exhibit remarkable properties.[28] For example, the strong correlation of itinerant electrons in VS_2 monolayer makes the $3d_z^2$ orbitals split into two bands and leads to 2D Stoner ferromagnetism.[29,30] With itinerant ferromagnetism, Fe_3GeTe_2 may open up a new chance to realize room-temperature ferromagnetism. Therefore, understanding the physical mechanism of ferromagnetism in Fe_3GeTe_2 would give rise to new 2D spintronic properties.

In this paper, a theoretical model is proposed to understand the magnetic interactions in 2D Fe_3GeTe_2, and the density functional theory (DFT) calculations are employed to evaluate the key parameters. We uncover the mechanism of magnetic anisotropy in maintaining the magnetic order of 2D systems. The model reveals a new form of long-range ferromagnetism and suggests a physical picture beyond the Stoner model. The Curie temperature of Fe_3GeTe_2 is then predicted by the model. Our theoretical model can also be applied to other 2D itinerant ferromagnetism systems.

2. Theory

In traditional theory, the Mermin–Wigner theorem[10] asserts that gapless excitation can occur in systems with con-

*Project supported by the Fundamental Research Funds for the Central Universities, China (Grant No. XJS200503) and the Post-Doctoral Research Project of Shaanxi Province, China.

†Corresponding author. E-mail: zzlin@xidian.edu.cn

© 2021 Chinese Physical Society and IOP Publishing Ltd

tinuous symmetry. In isotropic 2D systems, the gapless quasiparticle spectrum leads to a divergence of thermal distribution, which indicates the absence of magnetic order at finite temperature. However, anisotropic 2D systems hold low-energy gaps which protect the long-range magnetic order. To understand the magnetic order in Fe_3GeTe_2, let us start with the spin wave theory. The possible Heisenberg Hamiltonian in anisotropic 2D systems reads

$$H = -D\sum_i S_{iz}^2 - \lambda \sum_{ij\in 1^{\rm st}{\rm NN}} S_{iz}S_{jz} - J_1 \sum_{ij\in 1^{\rm st}{\rm NN}} \boldsymbol{S}_i\cdot\boldsymbol{S}_j - J_2 \sum_{ij\in 2^{\rm nd}{\rm NN}} \boldsymbol{S}_i\cdot\boldsymbol{S}_j. \quad (1)$$

Here, $\boldsymbol{S}_i$ denotes the spin of the local magnetic moment i. The single-atom anisotropy $D>0$ favors an off-plane easy axis. λ denotes the interatomic anisotropy between the first nearest neighbors ($1^{\rm st}$ NNs). J_1 is the Heisenberg couplings between $1^{\rm st}$ NNs, and J_2 is the Heisenberg couplings between the second nearest neighbors ($2^{\rm nd}$ NNs). To go beyond the classical approximation, the spins in Eq. (1) are now treated as quantum mechanical operators within the linear spin wave approximation (SWA). According to the Holstein–Primakoff representation,[31] the spin operators are expressed in terms of bosonic operators

$$S_i^+ = \sqrt{2S}\sqrt{1-\frac{b_i^+ b_i}{2S}}\,b_i, \quad (2)$$

$$S_i^- = \sqrt{2S}\,b_i^+\sqrt{1-\frac{b_i^+ b_i}{2S}}, \quad (3)$$

$$S_i^Z = S - b_i^+ b_i, \quad (4)$$

with b_i and b_i^+ the bosonic annihilation and creation operators on the site. Such representation leads to a complicated nonlinear Hamiltonian. SWA consists of only the quadratic terms in the bosonic operators b. Such approximation is valid for low-energy excitation, i.e., small occupations of the bosonic modes. By SWA, the Hamiltonian in Eq. (1) reads

$$H_{\rm SWA} = 2S(D+n_1\lambda+n_1J_1+n_2J_2)\sum_i b_i^+ b_i - 2J_1S\sum_{ij\in 1^{\rm st}{\rm NN}} b_i^+ b_j - 2J_2S\sum_{ij\in 2^{\rm nd}{\rm NN}} b_i^+ b_j, \quad (5)$$

where n_1 and n_2 are the numbers of $1^{\rm st}$ NNs and $2^{\rm nd}$ NNs, respectively. The $H_{\rm SWA}$ describes bosonic excitations moving in the lattice with on-site energy $\varepsilon_0 = 2S(D+n_1\lambda+n_1J_1+n_2J_2)$ and the hopping J_1S and J_2S. The energy bands of spin waves can then be reproduced by Eq. (5).

At zero temperature, all the local magnetic moments are perfectly arranged in the same direction, and the system energy $E_{\rm SWA}=0$. Under low temperatures, the bosonic excitations make the system transit to $E_{\rm SWA}\geq E_{\rm g}$. The spin wave band gap $E_{\rm g} = \varepsilon_0 - 2n_1J_1S - 2n_2J_2S = 2S(D+n_1\lambda)$ protects the magnetic order escaping from thermal disturbance. We expand the lower band spectrum around the energy minima to get $E_{\rm SWA}\approx E_{\rm g}+\rho k^2$. Every magnon carries one unit of magnetic moment. In the framework of SWA, the magnetization reads

$$M = S - \frac{A_0}{(2\pi)^2}\int_{\rm BZ}\frac{{\rm d}^2\boldsymbol{k}}{{\rm e}^{E_{\rm SWA}/k_{\rm B}T}-1}. \quad (6)$$

In the absence of magnetic anisotropy (i.e., $D=0$ and $\lambda=0$ which leads to $E_{\rm g}=0$), the integral goes

$$\int_{\rm BZ}\frac{{\rm d}^2\boldsymbol{k}}{{\rm e}^{E_{\rm SWA}/k_{\rm B}T}-1} \approx k_{\rm B}T\int_{\rm BZ}\frac{{\rm d}^2\boldsymbol{k}}{\rho k^2}\to\infty. \quad (7)$$

This divergence is consistent with the Mermin–Wagner theorem, indicating that 2D ferromagnetism cannot exist without magnetic anisotropy.

3. Model and computation

The 2D Fe_3GeTe_2 lattice (Fig. 1(a)) has hexagonal symmetry with the primitive cell belonging to the space group $P\bar{6}m2$. The Fe atoms in one primitive cell are located in two inequivalent Wyckoff sites. In each primitive cell, two Fe atoms are located at the same position in the 2D plane at different heights (atoms 1 and 2 in Fig. 1(b)). The last Fe atom (atoms 3 in Fig. 1(b)) is sandwiched between the two Te atoms. The neighboring Fe atoms 1 and 2 constitute a magnetic group. J_1 and J_2 denote its Heisenberg coupling with $1^{\rm st}$ NNs and $2^{\rm nd}$ NNs. The magnetization of Fe_3GeTe_2 lattice is mainly decided by these groups. The magnetic moments of atom 3 are then induced by the three adjacent groups (which is explained in supplementary section 3). In the following text, we treat each Fe atom group (composed of 1 and 2) as a whole magnetic object.

To evaluate the values of Heisenberg coupling and magnetic anisotropy, DFT calculations are performed with the projector augmented-wave method[32,33] and implemented in the Vienna *ab initio* simulation package.[34–37] The plane-wave basis with a kinetic energy cutoff of 400 eV is adopted. The convergence threshold is set to 10^{-5} eV for the energy difference between two successive iterations. Along the direction perpendicular to the Fe_3GeTe_2 plane, a vacuum layer of 12 Å is set up. We also test a kinetic energy cutoff of 500 eV with a vacuum layer of 16 Å, which results in a similar energy band profile and Heisenberg couplings J_1 and J_2. The exchange-correlation functional is treated within the local density approximation (LDA).[38] The correction of van der Waals interactions is treated by the DFT-D3 method with Becke–Jonson damping.[39,40] To calculate the magnetic anisotropy energy (MAE), the spin–orbit coupling is included in the computation with a full k-point grid. The Brillouin zone of 1×1 (6×1) supercell is sampled in $12\times12\times1$ ($2\times12\times1$) Monkhorst–Pack grid. The lattice structures are relaxed until all the atomic forces are below 0.001 eV/Å. The above calculation gives a lattice constant $a_0=3.89$ Å.

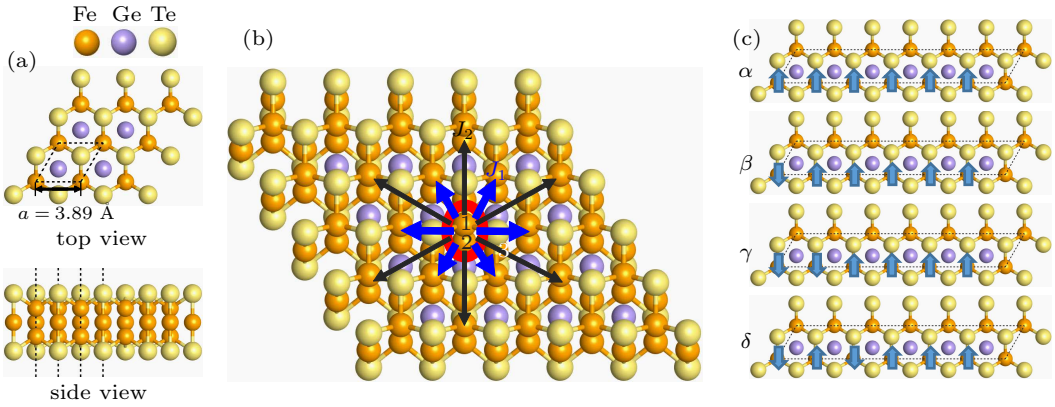


Fig. 1. Structure and magnetic coupling of Fe_3GeTe_2. (a) The structure of Fe_3GeTe_2 with the primitive cell shown by dashed lines. (b) The atomic group composed of atoms 1 and 2, and the coupling J_1 with 1st NNs and J_2 with 2nd NNs. (c) 6×1 supercell and four different configurations for the magnetization of the atomic groups. The arrows denote the directions of magnetic moments on the Fe atomic groups.

It is worth discussing the choice of DFT functional here. To verify the reliability of LDA, we also perform comparison calculations using the Perdew–Burke–Ernzerhof (PBE) functional[41] and the hybrid Heyd–Scuseria–Ernzerhof (HSE06) functional.[42,43] The LDA functional gives a magnetic moment $m = 4.55\mu_B$ per primitive cell, which is in the range of experimental values (m = 3.60–4.89 μ_B).[20,21] However, the obtained magnetic moments by the PBE ($m = 6.32\mu_B$) and HSE06 ($m = 7.11\mu_B$) functionals are drastically overestimated. The band structures (supplementary Fig. S1) show a feature of band shift in FM Fe_3GeTe_2 monolayer. The PBE or HSE06 functional present a larger band shift than LDA. The disagreement between theoretical (PBE or HSE06) and experimental magnetic moments also appears in the case of Fe-based superconductors.[44] This suggests that LDA, which is used throughout this work, is suitable to describe the electronic structure of Fe_3GeTe_2.

Within the Heisenberg model, the interatomic couplings are evaluated via the energy-mapping method.[45] A 6×1 supercell (Fig. 1(c)) is employed as a model. The configurations α, β, γ, and δ exhibit different magnetic moments on the Fe atomic groups. DFT calculations without SOC count the energy of Heisenberg coupling without magnetic anisotropy. According to the Heisenberg model, their energies read

$$E_\beta - E_\alpha = 16J_1S^2 + 24J_2S^2, \tag{8}$$

$$E_\gamma - E_\alpha = 16J_1S^2 + 32J_2S^2, \tag{9}$$

$$E_\delta - E_\alpha = 32J_1S^2 + 40J_2S^2. \tag{10}$$

Based on the DFT total energies without SOC, the Heisenberg coupling parameters J_1 and J_2 are obtained by the ordinary least squares method (see supplementary section 2).

4. Results and discussion

4.1. DFT calculations

The mission of DFT calculations is to obtain the spin S of the Fe atomic group and the parameters in Eq. (1) (D, λ, J_1 and J_2). LDA provides a total magnetic moment $m = 4.55$ μ_B per primitive cell, and the magnetic moment of the Fe atomic group is 3.58 μ_B. In DFT, the calculations of magnetic moments are based on atomic Wigner–Seitz radii, which are somewhat vague. Here we take an integral on the magnetic moment and can convince that $S = 2$ is the spin owing by the Fe atomic group.

Next, D and λ can be fitted from the MAE calculation. DFT calculations reveal that 2D Fe_3GeTe_2 monolayer is uniaxial with the easy axis along the z-direction perpendicular to the 2D surface. Based on the hexagonal symmetry of Fe_3GeTe_2, the MAE only depends on θ, which is the angle between lattice magnetization and the z axis.[46] According to Eq. (1), the MAE can be written as MAE $= (D + n_1\lambda)S^2\sin^2\theta$. On the other hand, the MAE of a hexagonal crystal can be fit into[46] MAE $\approx K\sin^2\theta$. DFT calculation results (Fig. 3(c)) fit $K = 2.46$ meV/cell. So we get $D + n_1\lambda \approx K/S^2 = 0.62$ meV.

By DFT total energies of the magnetic configurations in Fig. 1(c), Eqs. (8)–(10) provide a way to obtain J_1 and J_2. With a kinetic energy cutoff of 500 eV and a vacuum layer of 16 Å, DFT calculations obtain the energies $E_\beta - E_\alpha = 37.2$ meV, $E_\gamma - E_\alpha = 66.2$ meV, and $E_\delta - E_\alpha = 138.8$ meV. By the method in supplementary section 2, we finally get $J_1 = 1.21$ meV and $J_2 = -0.16$ meV (Fig. 1(b)).

4.2. Magnon spectrum

The magnon spectrum can be obtained from the spin wave Hamiltonian Eq. (5). The hexagonal Fe_3GeTe_2 has 1st NN and 2nd NN number $n_1 = 6$ and $n_2 = 6$. The Bloch Hamiltonian for the lattice reads

$$\begin{aligned} & E_{\mathrm{SWA}}(\boldsymbol{k}) \\ &= \varepsilon_0 - 2J_1S\sum_{j\in 1^{\mathrm{st}}\mathrm{NN\,of}\,i} \mathrm{e}^{\mathrm{i}\boldsymbol{k}\cdot\boldsymbol{R}_{ij}} - 2J_2S\sum_{j\in 2^{\mathrm{nd}}\mathrm{NN\,of}\,i} \mathrm{e}^{\mathrm{i}\boldsymbol{k}\cdot\boldsymbol{R}_{ij}} \\ &= \varepsilon_0 - 4J_1S\left[\cos k_x a + \cos\left(\frac{1}{2}k_x + \frac{\sqrt{3}}{2}k_y\right)a \right. \\ &\quad \left. + \cos\left(-\frac{1}{2}k_x + \frac{\sqrt{3}}{2}k_y\right)a\right] \end{aligned}$$

$$-4J_2S\Big[\cos\frac{\sqrt{3}}{2}(\sqrt{3}k_x+k_y)a + \cos\frac{\sqrt{3}}{2}(-\sqrt{3}k_x+k_y)a+\cos\sqrt{3}k_y a\Big]. \quad (11)$$

Here, $a = 3.89$ Å is the lattice constant, and the on-site energy $\varepsilon_0 = 2S(D+n_1\lambda+n_1J_1+n_2J_2) = 55.84$ meV (see Section 2) can be evaluated from the data in Subsection 4.1. Figure 2(a) plots $E_{\rm SWA}(\boldsymbol{k})$ along the high-symmetry lines of the Brillöuin zone. For a more visual plot, please see Fig. 2(b). We can see an energy gap $E_{\rm g} = 2S(D+n_1\lambda) = 2.46$ meV. This gap protects the magnetic order against thermal fluctuation and makes it survive at finite temperature.

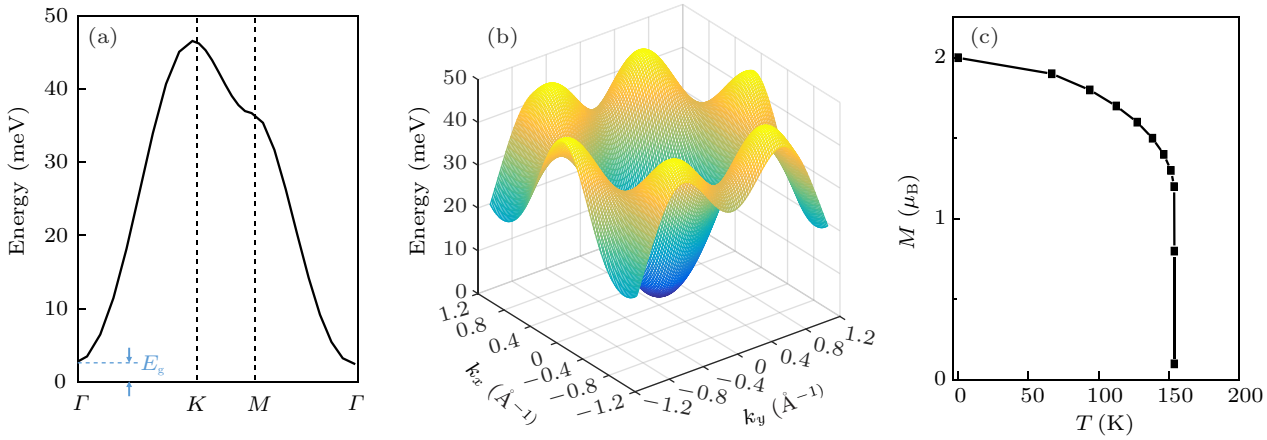


Fig. 2. Magnon spectrum and the Curie temperature. (a) The energy spectrum of spin wave magnon. (b) Three-dimensional plot of the magnon spectrum. (c) The magnetic moment of one primitive cell versus temperature T.

4.3. Curie temperature

We now provide a rough estimate of the Curie temperature based on nonlinear spin wave theory. We use the expressions Eqs. (2) and (3) for spin operators, and expand them to fourth order in the bosonic operators

$$S_i^+ \approx \sqrt{2S}\left(1-\frac{b_i^+b_i}{4S}\right)b_i, \quad (12)$$

$$S_i^- \approx \sqrt{2S}b_i^+\left(1-\frac{b_i^+b_i}{4S}\right). \quad (13)$$

At intermediate temperatures, there is a finite number of spin waves that are accounted for the high-order terms in bosonic operators when substituting the previous expansion in the spin Hamiltonian. The spin Hamiltonian contains four field operators and therefore is not rigorously solvable. Here, the effect of the spin wave population in the Hamiltonian is described by the substitution

$$\begin{aligned} b_i^+b_ib_j^+b_j &= (\langle b_i^+b_i\rangle + C_i)(\langle b_j^+b_j\rangle + C_j) \\ &= \langle b_i^+b_i\rangle b_j^+b_j + b_i^+b_i\langle b_j^+b_j\rangle - \langle b_i^+b_i\rangle\langle b_j^+b_j\rangle + C_iC_j \\ &\to \langle b_i^+b_i\rangle b_j^+b_j + b_i^+b_i\langle b_j^+b_j\rangle. \end{aligned} \quad (14)$$

Here C_i is the perturbation terms. The last step removes the constant term (do not affect the physics of Hamiltonian) and ignores the high-order perturbation. Using a mean-field approximation, we have

$$\begin{aligned} S_i^ZS_j^Z &= (S-b_i^+b_i)(S-b_j^+b_j) \\ &= S^2 - S(b_i^+b_i+b_j^+b_j) + b_i^+b_ib_j^+b_j \\ &\to -(S-\langle b^+b\rangle)(b_i^+b_i+b_j^+b_j). \end{aligned} \quad (15)$$

By Eqs. (12) and (13) we have

$$S_i^+S_j^- \to 2Sb_ib_j^+\left(1-\frac{\langle b^+b\rangle}{S}\right), \quad (16)$$

$$S_i^-S_j^+ \to 2Sb_i^+b_j\left(1-\frac{\langle b^+b\rangle}{S}\right). \quad (17)$$

The above formulas result in a substitution $DS \to DM$, $\lambda S \to \lambda M$, $J_1S \to J_1M$, and $J_2S \to J_2M$ in the Hamiltonian $H_{\rm SWA}$. So, the magnetization is expressed by a self-consistent equation

$$M(T) = S - \frac{A_0}{(2\pi)^2}\int_{\rm BZ}\frac{{\rm d}^2\boldsymbol{k}}{{\rm e}^{M(T)E_{\rm SWA}(\boldsymbol{k})/Sk_{\rm B}T}-1}. \quad (18)$$

At a given temperature T, the magnetization $M(T)$ can then be derived by numerically solving this equation. This equation implies that the temperature T reduces quasiparticle energy and decreases the low-energy gap of magnon. The effect destroys the magnetic order in the system. The numerical results are shown in Fig. 2(c). $M(T)$ drastically decreases with increasing temperature when $T > 100$ K. According to the results, we get a Curie temperature $T_{\rm c} = 154$ K. In a recent experiment,[18] the magnetic hysteresis of monolayer and bilayer Fe_3GeTe_2 is detected to vanish at $T = 100$ K. People also used polar refractive magnetic circular dichroism microscopy to measure layer-dependent $T_{\rm c}$ of Fe_3GeTe_2 and detected a Curie temperature of about 70 K with a size of 2 μm.[18] These experiment results are generally consistent with our calculation.

4.4. Stoner ferromagnetism

Fe_3GeTe_2 monolayer is metallic with a non-integer magnetic moment. This inspires us to apply the Stoner model to understand the mechanism of yielding the magnetic order. The DFT bands of Fe_3GeTe_2 monolayer (Fig. 3(a)) show a feature of band shift. The shapes of corresponding spin-up and spin-down bands are similar. The spin-up band has lower energy, while the spin-down band has higher energy. From the density of states (DOS) (Fig. 3(b)), we can see that the electron states near the Fermi level are mainly contributed by Fe 3d orbitals. To calculate the average band splitting Δ near the Fermi level, five corresponding bands (bold lines in Fig. 3(a)) are chosen. Their average energy gap is $\Delta = 1.17$ eV. According to the Stoner model,[47] we have $\Delta = Um_0$, where $m_0 = m/3 = 1.52\ \mu_B$ is the average magnetic moment per Fe atom. Then the Hubbard $U = 0.77$ eV is determined. It is worth noting that this U is the result of electron interactions within LDA, which does not have to add it into LDA (if U is added to LDA, the exchange-correlation is stronger and that results in a band profile more close to PBE (see supplementary Fig. S1(d)) and a larger magnetic moment m). By spin-non-polarized DFT calculations, we obtain a DOS $D_{NM}(E_F) = 1.76$ states/eV/atom at the Fermi level of non-magnetic (NM) Fe_3GeTe_2 monolayer. Finally, the Stoner criterion, i.e., $UD_{NM}(E_F) = 1.36 > 1$, is examined to establish. This criterion reveals that the ferromagnetism of Fe_3GeTe_2 monolayer is spontaneous. To further consider the influence of magnetic anisotropy, SOC is added to the calculation of Hubbard U. For the magnetization angle $\theta = 0°$–$90°$, $U = 0.78$–0.77 eV, which changes only by 1%. Thus, the SOC has little effect on the electron correlation. The magnetic anisotropy should arise from the energy difference of the crystal field acting on the itinerant electrons with different magnetization directions.

To understand the formation of ferromagnetism in Fe_3GeTe_2, we further analyze the mechanism by the Stoner model. When a rigid band splitting Δ happens in NM Fe_3GeTe_2 (Fig. 3(d)), the spin-up electron number $n_\uparrow$ is then larger than the spin-down electron number $n_\downarrow$, for which their sum $n_\uparrow + n_\downarrow = n$ should be a constant and equal to the total electron number. By the DOS of NM Fe_3GeTe_2, the electron numbers per Fe atom can be counted as

$$n_\uparrow = \frac{1}{2}\int_0^{E_F+\frac{\Delta}{2}} D_{NM}(E)\,dE, \tag{19}$$

$$n_\downarrow = \frac{1}{2}\int_0^{E_F-\frac{\Delta}{2}} D_{NM}(E)\,dE. \tag{20}$$

Then we express the magnetic moment per atom as $m_0(\Delta) = n_\uparrow - n_\downarrow$, by which an inverse function $\Delta = \Delta(m_0)$ can be obtained numerically. On the other hand, the band splitting Δ is decided by the Hubbard model. On every Fe atom, the repulsion between spin-up and spin-down electrons in 3d orbitals leads to an energy difference of single quasiparticle, i.e.,

$$\varepsilon_\downarrow(\boldsymbol{k}) - \varepsilon_\uparrow(\boldsymbol{k}) = U(n_\uparrow - n_\downarrow). \tag{21}$$

Then the band splitting reads $\Delta = U(n_\uparrow - n_\downarrow) = Um_0$. The above two equations, $\Delta = \Delta(m_0)$ and $\Delta = U(n_\uparrow - n_\downarrow) = Um_0$, are plotted in Fig. 3(d) with increasing m_0. It can be seen that they have a trivial intersection $m_0 = 0$ and a non-trivial intersection $m_0 = 1.9$ which is close to the previous DFT calculation ($m_0 = 1.52$). The above analysis provides an understanding of the spontaneous magnetization in Fe_3GeTe_2.

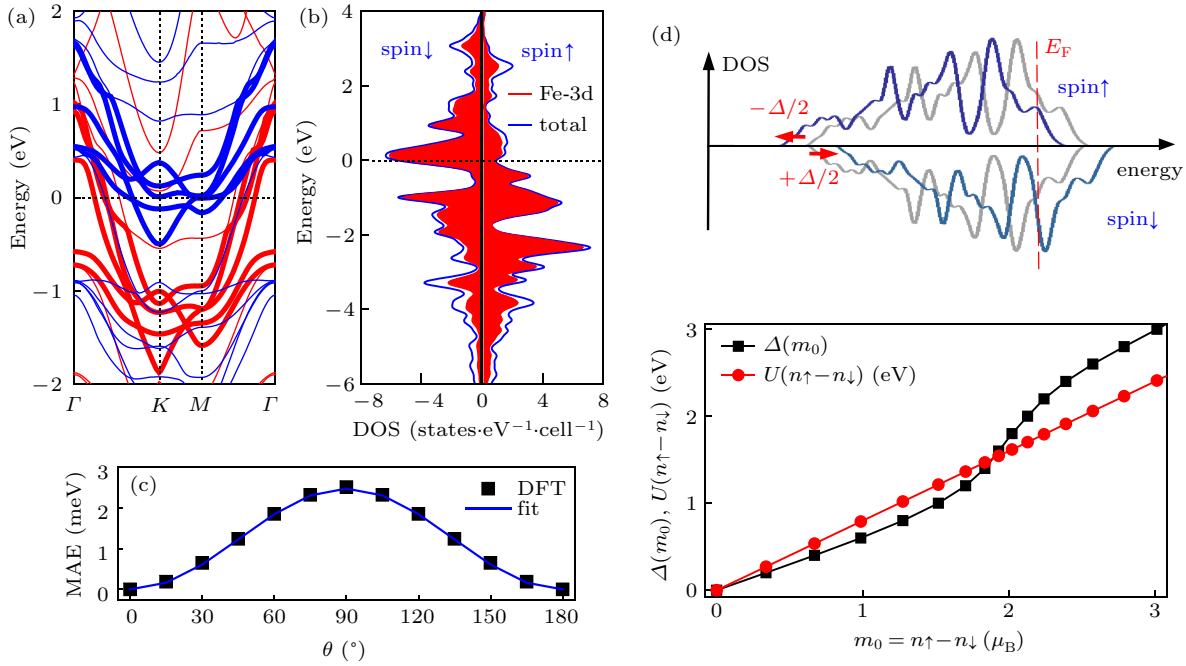


Fig. 3. (a) Spin-resolved band structure of Fe_3GeTe_2 monolayer without SOC. Red (blue) lines denote spin-up (spin-down) bands. (b) DOS of Fe_3GeTe_2 monolayer. (c) MAE of Fe_3GeTe_2 monolayer. (d) Band shift and the Stone criterion.

5. Conclusion

In this work, we attempt to unravel the origin of 2D ferromagnetism in Fe_3GeTe_2 monolayer. By combining the theoretical model and DFT simulations, a physical picture is built to describe the magnetic interactions in 2D Fe_3GeTe_2. DFT calculations are employed to evaluate the Heisenberg coupling and magnetic anisotropy. The model reveals long-range ferromagnetic order in 2D systems should be maintained by magnetic anisotropy. The predicted Curie temperature agrees with a recent experiment. The Stoner model provides an insight into the spontaneous magnetization in Fe_3GeTe_2 and results in a prediction close to DFT calculations. Our model is successful in understanding the magnetization mechanism in 2D Fe_3GeTe_2. In future studies, the model can be extended to other 2D systems.

References

[1] Huang B, Clark G, Navarro-Moratalla E, Klein D R, Cheng R, Seyler K L, Zhong D, Schmidgall E, McGuire M A, Cobden D H, Yao W, Xiao D, Jarillo-Herrero P and Xu X D 2017 *Nature* **546** 270

[2] Pan L, Wen H, Huang L, Chen L, Deng H X, Xia J B and Wei Z 2019 *Chin. Phys. B* **28** 107504

[3] Zhao L S, Chen C P, Liu L L, Yu H X, Chen Y and Wang X C 2018 *Chin. Phys. B* **27** 016301

[4] Kang K, Lee K H, Han Y, Gao H, Xie S, Muller D A and Park J 2017 *Nature* **550** 229

[5] Li M Y, Shi Y, Cheng C C, Lu L S, Lin Y C, Tang H L, Tsai M L, Chu C W, Wei K H, He J H, Chang W H, Suenaga K and Li L J 2015 *Science* **349** 524

[6] Ribeiro-Palau R, Zhang C, Watanabe K, Taniguchi T, Hone J and Dean C R 2018 *Science* **361** 690

[7] Xu W, Liu W, Schmidt J F, Zhao W, Lu X, Raab T, Diederichs C, Gao W, Seletskiy D V and Xiong Q 2017 *Nature* **541** 62

[8] Yu Z, Ong Z Y, Li S, Xu J B, Zhang G, Zhang Y W, Shi Y and Wang X 2017 *Adv. Func. Mat.* **27** 1604093

[9] Yuan J H, Chen N, Mo H, Zhang Y and Zhang Z H 2016 *Chin. Phys. Lett.* **33** 037302

[10] Mermin N D and Wagner H 1966 *Phys. Rev. Lett.* **17** 1133

[11] Jiang P, Wang C, Chen D, Zhong Z, Yuan Z, Lu Z Y and Ji W 2019 *Phys. Rev. B* **99** 144401

[12] Kim H H, Yang B, Patel T, Sfigakis F, Li C, Tian S, Lei H and Tsen A W 2018 *Nano Lett.* **18** 4885

[13] Song T, Cai X, Tu M W Y, Zhang X, Huang B, Wilson N P, Seyler K L, Zhu L, Taniguchi T, Watanabe K, McGuire M A, Cobden D H, Xiao D, Yao W and Xu X 2018 *Science* **360** 1214

[14] Wang Z, Gutierrez-Lezama I, Ubrig N, Kroner M, Gibertini M, Taniguchi T, Watanabe K, Imamoglu A, Giannini E and Morpurgo A F 2018 *Nat. Commun.* **9** 2516

[15] Sivadas N, Okamoto S, Xu X, Fennie C J and Xiao D 2018 *Nano Lett.* **18** 7658

[16] Gong C, Li L, Li Z, Ji H, Stern A, Xia Y, Cao T, Bao W, Wang C, Wang Y, Qiu Z Q, Cava R J, Louie S G, Xia J and Zhang X 2017 *Nature* **546** 265

[17] Zhang J, Cai X, Xia W, Liang A, Huang J, Wang C, Yang L, Yuan H, Chen Y, Zhang S, Guo Y, Liu Z and Li G 2019 *Phys. Rev. Lett.* **123** 047203

[18] Deng Y, Yu Y, Song Y, Zhang J, Wang N Z, Sun Z, Yi Y, Wu Y Z, Wu S, Zhu J, Wang J, Chen X H and Zhang Y 2018 *Nature* **563** 94

[19] Wang Z, Sapkota D, Taniguchi T, Watanabe K, Mandrus D and Morpurgo A F 2018 *Nano Lett.* **18** 4303

[20] Chen B, Yang J, Wang H, Imai M, Ohta H, Michioka C, Yoshimura K and Fang M 2013 *J. Phys. Soc. Jpn.* **82** 124711

[21] Deiseroth H J, Aleksandrov K, Reiner C, Kienle L and Kremer R K 2006 *Eur. J. Inorg. Chem.* **8** 1561

[22] May A F, Calder S, Cantoni C, Cao H and McGuire M A 2016 *Phys. Rev. B* **93** 014411

[23] Tian C K, Wang C, Ji W, Wang J C, Xia T L, Wang L, Liu J J, Zhang H X and Cheng P 2019 *Phys. Rev. B* **99** 184428

[24] Fei Z Y, Huang B, Malinowski P, Wang W B, Song T C, Sanchez J, Yao W, Xiao D, Zhu X Y, May A F, Wu W D, Cobden D H, Chu J H and Xu X D 2018 *Nat. Mater.* **17** 778

[25] Liu S, Yuan X, Zou Y, Sheng Y, Huang C, Zhang E, Ling J, Liu Y, Wang W, Zhang C, Zou J, Wang K and Xiu F 2017 *npj 2D Mat. Appl.* **1** 30

[26] Zheng G, Xie W Q, Albarakati S, Algarni M, Tan C, Wang Y, Peng J, Partridge J, Farrar L, Yi J, Xiong Y, Tian M, Zhao Y J and Wang L 2020 *Phys. Rev. Lett.* **125** 047202

[27] Onsager L 1944 *Phys. Rev.* **65** 117

[28] Fazekas P 1999 *Lecture Notes on Electron Correlation and Magnetism* (Singapore: World Scientific)

[29] Isaacs E B and Marianetti C A 2016 *Phys. Rev. B* **94** 035120

[30] Zhuang H L and Hennig R G 2016 *Phys. Rev. B* **93** 054429

[31] Holstein T and L P H 1940 *Phys. Rev.* **58** 1098

[32] Kresse G and Joubert D 1999 *Phys. Rev. B* **59** 1758

[33] Blöchl P E 1994 *Phys. Rev. B* **50** 17953

[34] Kresse G and Furthmüller J 1996 *Phys. Rev. B* **54** 11169

[35] Kresse G and Furthmüller J 1996 *Comp. Mat. Sci.* **6** 15

[36] Kresse G and Hafner J 1993 *Phys. Rev. B* **47** 558

[37] Kresse G and Hafner J 1994 *Phys. Rev. B* **49** 14251

[38] Perdew J P and Zunger A 1981 *Phys. Rev. B* **23** 5048

[39] Grimme S, Antony J, Ehrlich S and Krieg H 2010 *J. Chem. Phys.* **132** 154104

[40] Grimme S, Ehrlich S and Goerigk L 2011 *J. Comp. Chem.* **32** 1456

[41] Perdew J P, Burke K and Ernzerhof M 1996 *Phys. Rev. Lett.* **77** 3865

[42] Heyd J, Scuseria G E and Ernzerhof M 2003 *J. Chem. Phys.* **118** 8207

[43] Heyd J, Scuseria G E and Ernzerhof M 2006 *J. Chem. Phys.* **124** 219906

[44] Singh D J and Du M-H 2008 *Phys. Rev. Lett.* **100** 237003

[45] Xiang H, Lee C, Koo H J, Gong X and Whangbo M H 2013 *Dalton Trans.* **42** 823

[46] O'Handley R C 1999 *Modern Magnetic Materials: Principles and Applications* (Wiley-Interscience, 1st ed.).

[47] Blundell S 2001 *Magnetism in Condensed Matter* (New York: Oxford University Press)